Adsorption Kinetics and Size Exclusion Properties of Probe Molecules for the Selective Porosity in a Carbon Molecular Sieve Used for Air Separation

ARTICLE *in* THE JOURNAL OF PHYSICAL CHEMISTRY B · OCTOBER 2001

Impact Factor: 3.3 · DOI: 10.1021/jp0108263

2 AUTHORS, INCLUDING:

Keith Mark Thomas
Newcastle University
197 PUBLICATIONS **10,104** CITATIONS

SEE PROFILE

Adsorption Kinetics and Size Exclusion Properties of Probe Molecules for the Selective Porosity in a Carbon Molecular Sieve Used for Air Separation

C. R. Reid and K. M. Thomas*

Northern Carbon Research Laboratories, Department of Chemistry, Bedson Building, University of Newcastle upon Tyne, Newcastle upon Tyne, NE1 7RU, U.K.

Received: March 5, 2001; In Final Form: July 12, 2001

The adsorption characteristics of a series of planar (ethylene, benzene, and pyridine) and tetrahedral (methane, chloromethane, dichloromethane, chloroform, and carbon tetrachloride) molecules on a carbon molecular sieve used for air separation (CMS A) were investigated over a range of temperatures as a function of pressure, to study the selective porosity. The size-exclusion characteristics of planar and tetrahedral molecules indicate that the selective porosity behaves as though it has spherical-shaped structural characteristics and, therefore, two minimum dimensions need to be considered in relation to size exclusion. The partial exclusion of the probe molecule adsorptives from the microporous structure for sizes >360 pm allowed the selective and nonselective microporosity and the meso/macroporosity to be quantified. Adsorption kinetics obey a linear-driving-force mass transfer, combined barrier resistance/diffusion, or Fickian kinetic models depending on the adsorptive and experimental conditions. Comparison of the results with previous studies of the adsorption of linear and spherical molecules on CMS A show that a decrease in the adsorption rate constant of ∼ 4 orders of magnitude was observed for an increase in molecular size over the range ∼290−420 pm. The activation energies and preexponential factors for the adsorption kinetics and the isosteric heats of adsorption are discussed in terms of the structural characteristics of the adsorptives and the adsorption mechanism.

Introduction

Carbon molecular sieves (CMS) are microporous materials with a relatively high adsorption capacity and kinetic selectivity for a range of gases that are used widely for the separation of air into its components.[1−3] The kinetic selectivity is produced by carbon deposition on a nonselective microporous substrate to give selective porosity, which is distributed heterogeneously within the carbon microporous structure. The heterogeneous distribution of the selective porosity is apparent when CMS pellets are reduced in particle size and the kinetic selectivity is lost because of the introduction of nonselective adsorption pathways.[3] Therefore, only part of the microporous material has kinetic selectivity and, hence, molecular sieving characteristics. It is generally accepted that the selective porosity has dimensions similar to the adsorbate and the diffusing molecule experiences a net repulsive force on entering the selective porosity.[4,5] Therefore, the molecule must pass over an energy barrier during diffusion through the kinetically selective porosity and this leads to differences in the adsorption kinetics for various gases/vapors. This difference in adsorption kinetics for oxygen and nitrogen is the basis for the separation of air by the pressure swing adsorption process.

The heterogeneous distribution of the selective porosity produced by carbon deposition within the carbon microporous structure makes it very difficult to characterize the selective porosity, which is of fundamental importance in assessing the gas separation characteristics of the CMS.[3,6−8] The limited information available on the variation of kinetic selectivity with extent of carbon deposition indicated that for the CMS studied, the rates of adsorption of both oxygen and nitrogen decreased with increasing extent of carbon deposition, whereas the ratios of the rates were not changed greatly.[9] It has been proposed that the difference in the adsorption kinetics of these two gases is mainly related to molecular size, with the kinetic diameter of N_2 (364 pm) being slightly larger than that of O_2 (346 pm)[1] since adsorbate/adsorbent interactions generally increase with increasing adsorbate size. However, there are also shape-dependent factors for nonspherical molecules, which may influence the adsorption process. Studies of the adsorption of noble gases[6] and linear adsorptives[8] indicate that factors such as specific adsorbate/adsorbent interactions also influence the adsorption kinetics. The adsorptive dimensions do not provide a good indication of the adsorption kinetics for a wide range of adsorptives.[6,8] Previous studies of a limited number of gases have involved the calculation of critical pore dimensions, where the pore dimensions give zero interaction potentials for the adsorptive, to assess the relative orders of the rates of adsorption for a range of adsorptives.[4,5] These critical dimensions appear to provide a better correlation for adsorption kinetics than comparison of the adsorptive dimensions for the limited data available.[4,5]

The selective porosity in the heterogeneous CMS provides a barrier to the diffusion of a range of adsorptives into the porous structure and in the case of larger molecules, may lead to exclusion of the adsorptive from part of the porous structure. In this study, the adsorption characteristics of planar and tetrahedral probe molecules have been investigated as a function of temperature and pressure to determine the relative importance of factors such as molecular size and shape in determining the adsorption kinetic and size-exclusion characteristics. The results are compared with previous studies of spherical and linear adsorptives and discussed in terms of the mechanism of adsorption in carbon molecular sieve materials and the structure

* To whom correspondence should be addressed. E-mail: mark.thomas@ncl.ac.uk.

10.1021/jp0108263 CCC: $20.00
Published on Web 10/06/2001

of the selective porosity. The molecular dimensions of the adsorptives have been compared with the size-exclusion characteristics of the CMS adsorbent and the pore size distribution of the selective porosity inferred. The activation energies and preexponential factors for diffusion through the selective porosity and isosteric heats of adsorption have been determined and are discussed in relation to the adsorption mechanism.

Experimental Section

Materials Used. The commercial carbon molecular sieve (CMS A) used in this study was supplied by Air Products and Chemicals Inc., Allenton, U.S. The CMS was prepared by carbon deposition on a microporous substrate. The gases used were supplied by BOC Ltd, London, U.K., and had the following purities: methane (99.995%), chloromethane (99.9%), and ethylene (99.92%). Dichloromethane (99.9%), chloroform (99.9%), carbon tetrachloride (99.9%), benzene (99.9%), and pyridine (99.9%) were obtained from Aldrich Chemicals, U.K.

Measurement of Adsorption Kinetics. The kinetic measurements were carried out using an Intelligent Gravimetric Analyzer (IGA) supplied by Hiden Analytical Ltd. The instrument is an ultrahigh vacuum system with a fully computerized microbalance, which allows the adsorption/desorption isotherms and the corresponding kinetics of adsorption or desorption for each pressure step to be determined with the approach to equilibrium being monitored in real time using a computer algorithm.[6−8,10] The condition for achieving equilibrium was 99% of the predicted value calculated in real time using the uptake profile. The balance and pressure control system were fully thermostatted to 0.2 K to eliminate the effects of changes in the external environment. The microbalance had a long-term stability of ± 1 μg with a weighing resolution of 0.2 μg. The carbon sample (∼0.5 g) was outgassed to a constant weight at 343 K and 10^{-5} Pa prior to measurement of the isotherms. The pressure was monitored by three pressure transducers with ranges of 0−0.2 kPa, 0−10 kPa, and 0−1 MPa. The liquid used to generate the vapor was degassed fully by repeated evacuation and vapor equilibration cycles of the liquid supply side of the vapor reservoir. The vapor pressure was gradually increased, over a time-scale of ∼30 s, to prevent disruption of the microbalance, until the desired value was achieved. Therefore, the period over which the pressure change occurred was very small compared with the adsorption kinetics. The accuracy of the set-point pressure regulation was ± 0.02% of the range used. The pressure was maintained at the set point by active computer control of inlet/outlet valves throughout the duration of the kinetic experiments. The sample temperature was measured at ∼5 mm from the sample and was controlled to ± 0.05 K throughout the duration of the experiment by circulation of 1:1 ethylene glycol/water mixture from a computer-controlled liquid circulation bath. The initial pressure increment from high vacuum ($<10^{-5}$ Pa) resulted in a change of temperature of 0.5 K resulting from the introduction of conduction from the thermostatically controlled water jacket through the gas to the sample. The isotherms were typically repeatable to better than ±1%. In the case of chloromethane adsorption, the kinetics were so slow that the experiments had to be carried out at a temperature, which could not be achieved by the circulating liquid method. In this case, a furnace was used to achieve the desired temperature and this resulted in lower sample temperature stability (±0.3 K).

The saturated vapor pressures were calculated using the following equation:[11,12]

$$\log_{10} p = A - \frac{B}{T + C} \qquad (1)$$

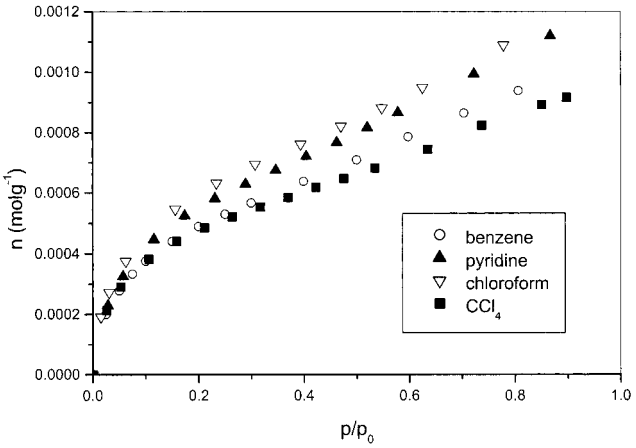

Figure 1. Adsorption isotherms for chloroform, carbon tetrachloride, benzene and pyridine at 303 K on a p/p^0 basis: benzene (○); pyridine (▲); chloroform (▽); carbon tetrachloride (■).

where p is the saturated vapor pressure (Torr), T is the temperature in degrees Celsius and A, B, and C are constants defined by the adsorbate: chloromethane: $A = 7.09349$, $B = 948.58$, $C = 249.34$; dichloromethane: $A = 7.4092$, $B = 1325.9$, $C = 252.6$; chloroform: $A = 6.4934$, $B = 929.44$, $C = 196.03$; carbon tetrachloride: $A = 6.87926$, $B = 1212.021$, $C = 226.41$, benzene: $A = 6.90565$, $B = 1211.033$, $C = 220.790$; pyridine: $A = 7.04115$, $B = 1373.8$, $C = 214.98$.

Results

Adsorption Capacities. The adsorption isotherms of a range of tetrahedral and planar adsorptives were investigated for comparison with previous studies of linear[8] and spherical[6] adsorptives. Adsorption isotherms of methane, ethylene, chloroform, carbon tetrachloride, benzene, and pyridine are shown in Supporting Information. The adsorption of ethylene on CMS A was studied over the temperature range 303−343 K while methane adsorption was studied over the temperature range 338−358 K. An initial pressure increment of 0−50 kPa was used in both cases because of the relatively slow adsorption kinetics at low surface coverage. The faster adsorption rates at higher surface coverage allowed isotherms to be obtained on an acceptable time scale. However, the adsorption kinetics of chloroform, carbon tetrachloride, benzene, and pyridine on CMS A were much faster than either methane or ethylene, even though the molecules are larger. Therefore, these adsorptives were studied over the temperature range 273−323 K. The adsorption temperatures used in this study were well above the critical temperatures for ethylene and methane while chloroform, carbon tetrachloride, benzene, pyridine, and chloromethane were below their critical temperatures. A comparison of the adsorption isotherms for each vapor over the temperature range studied on a relative pressure basis showed that there was excellent agreement for each adsorptive. The adsorption isotherms for chloroform, carbon tetrachloride, benzene, and pyridine were type II in the IUPAC classification scheme.[13] A comparison on a relative pressure (p/p^0) basis is shown in Figure 1 and this shows the similarities in the isotherms. The total pore volumes were obtained by extrapolation of the isotherm data to $p/p^0 = 1$. The average total pore volumes for the temperature range studied, calculated using densities[11] of 1.4832, 1.594, 0.8736, and 0.9819 g cm^{-3} for chloroform, carbon tetrachloride, benzene, and pyridine respectively, were: chloroform (0.106 cm^3 g^{-1}), carbon tetrachloride (0.098 cm^3 g^{-1}), benzene (0.102 cm^3 g^{-1}), and pyridine (0.100 cm^3 g^{-1}). It is apparent from these

TABLE 1: Henry's Law and Virial Parameters for Gases and Vapors Adsorbed on CMS A

temp/K	chloroform	carbon tetrachloride	pyridine	benzene	ethylene	methane
			A_0/mol g^{-1} Pa^{-1}			
	0−30 kPa	0−25 kPa	0−5 kPa	0−15 kPa	0−100 kPa	0−100 kPa
273	−12.195 ± 0.039	−11.732 ± 0.067	−10.254 ± 0.095	−	−	−
283	−12.840 ± 0.062	−12.634 ± 0.027	−11.044 ± 0.084	−12.576 ± 0.016	−	−
293	−13.409 ± 0.137	−13.119 ± 0.051	−11.708 ± 0.053	−13.120 ± 0.037	−	−
303	−14.191 ± 0.046	−13.802 ± 0.053	−12.301 ± 0.041	−13.769 ± 0.034	−13.513 ± 0.272	−
313	−14.665 ± 0.058	−14.163 ± 0.041	−12.978 ± 0.043	−14.343 ± 0.028	−14.258 ± 0.066	−
323	−	−	−	−14.774 ± 0.037	−14.854 ± 0.027	−
333	−	−	−	−	−15.345 ± 0.055	−
338	−	−	−	−	−	−18.751 ± 0.007
343	−	−	−	−	−15.860 ± 0.058	−18.838 ± 0.002
348	−	−	−	−	−	−18.977 ± 0.017
353	−	−	−	−	−	−19.091 ± 0.011
358	−	−	−	−	−	−19.219 ± 0.016
			A_1/(g mol^{-1})			
	0−30 kPa	0−25 kPa	0−5 kPa	0−15 kPa	0−100 kPa	0−100 kPa
273	−3737 ± 78	−4919 ± 144	−3112 ± 159	−	−	−
283	−3714 ± 125	−4436 ± 60	−3000 ± 142	−3705 ± 35	−	−
293	−3768 ± 245	−4582 ± 112	−3049 ± 92	−3969 ± 83	−	−
303	−3322 ± 95	−4294 ± 113	−3105 ± 76	−3903 ± 82	−2480 ± 165	−
313	−3420 ± 129	−4540 ± 101	−2937 ± 88	−3808 ± 74	−2258 ± 44	−
323	−	−	−	−3843 ± 93	−2083 ± 19	−
333	−	−	−	−	−2004 ± 44	−
338	−	−	−	−	−	−899 ± 18
343	−	−	−	−	−1821 ± 50	−969 ± 5
348	−	−	−	−	−	−986 ± 55
353	−	−	−	−	−	−936 ± 38
358	−	−	−	−	−	−916 ± 59

results that there are no significant differences between the total pore volumes measured with tetrahedral and planar adsorptives, and Gurvitch's rule[13] is obeyed. Furthermore, the total pore volumes are significantly lower than the micropore volumes obtained previously from studies[8] of the adsorption of carbon dioxide, nitrous oxide, and acetylene at pressures up to 100 kPa. The adsorption of carbon dioxide at 273 K was also studied up to 900 kPa to obtain a more accurate value for the micropore volume. The results indicate that the four adsorptives are excluded to similar extents from part of the microporous structure of CMS A.

The adsorption rates were very slow for both chloromethane and dichloromethane. Therefore, only a single isotherm was obtained for chloromethane adsorption at 391 K (critical temperature 416 K) for comparison with other adsorptives on a p/p^0 basis to establish whether exclusion from the porous structure occurred. However, the pressure limit of the equipment did not allow the measurement of a full isotherm up to $p/p^0 = 1$ at this temperature, while the slow adsorption kinetics at low surface coverage led to the use of an initial pressure step of 0−50 kPa in order to carry out measurements on a reasonable time scale. In the case of dichloromethane adsorption, the kinetics were very slow and it was not possible to achieve equilibrium for a single step.

A virial equation approach was used to compare the isotherms when the adsorptives, for example, methane, ethylene etc. were above their critical temperatures. The virial equation can be written in the form

$$\ln(n/p) = A_0 + A_1 n + A_2 n^2 \text{ - - -} \qquad (2)$$

where n is the amount adsorbed at pressure p, and the first virial coefficient, A_0, is related to the Henry's law constant K_0 by the equation $K_0 = \exp(A_0)$.[14] K_0 is dependent on the interaction between the adsorbent surfaces and the adsorbed gas molecules. In this study, analysis of the data showed that the higher terms (A_2 etc.) in the virial equation could be ignored under conditions of low surface coverage. Virial analyses of the isotherms were also carried out when the adsorption took place below the critical temperatures of adsorptives for comparison with supercritical conditions. The virial graphs for chloroform adsorption are shown in Figure 2. The virial graphs for all the adsorptives studied were clearly linear at low surface coverage and the virial parameters obtained from these graphs are shown in Table 1. The virial graphs for carbon tetrachloride, benzene, and pyridine were similar. The values of the first virial coefficient (A_0) reflect adsorbate/adsorbent interaction, whereas the second virial parameter (A_1) is a function of adsorbate/adsorbate interactions. The value of A_1 for the gases/vapors studied were in the range ~ -900 to -5000 g mol^{-1} over the temperature range studied with only weak trends with temperature. The A_1 virial parameters for chloroform (-3322 to -3768 g mol^{-1}), carbon tetrachloride (-4294 to -4919 g mol^{-1}), benzene (-3705 to -3969 g mol^{-1}) and pyridine (-2937 to -3112 g mol^{-1}) were higher than for ethylene (-1821 to -2480 g mol^{-1}) and methane (-899 to

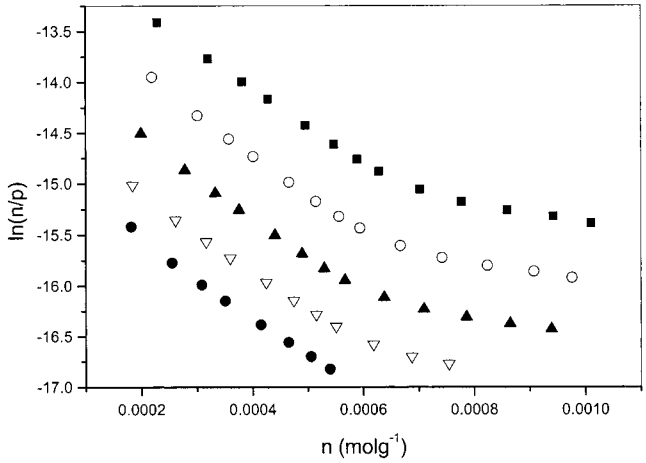

Figure 2. Virial graphs for the adsorption of benzene on carbon molecular sieve CMS A: Temperature range 283−323 K (283 K (■), 293 K (○), 303 K (▲), 313 K (▽), 323 K (●)).

TABLE 2: Comparison of Isosteric Enthalpies (kJ mol^{-1}) of Adsorption at Zero Surface Coverage Obtained from Determination of the Henry's Law Constant (K_0)

gas	Q_{st} (this work)[a]	Q_{st} refs 29−34	ΔH_{vap298} ref 11
methane	23.8 ± 1.1	12.2−12.7[b]	8.19[c]
ethylene	50.1 ± 1.5	17.99[b]	13.53[c]
chloroform	44.7 ± 1.6	37.2	31.28
carbon tetrachloride	44.1 ± 2.8	35.6−40.2	32.43
pyridine	47.6 ± 0.9	45.2	40.21
benzene	41.8 ± 1.5	42.7	33.83

[a] From the virial equation graphs with literature values and enthalpies of vaporization. [b] Refs 31 and 32 (adsorption on graphitized carbon blacks). [c] $\Delta H_{vap}(T_b)$.

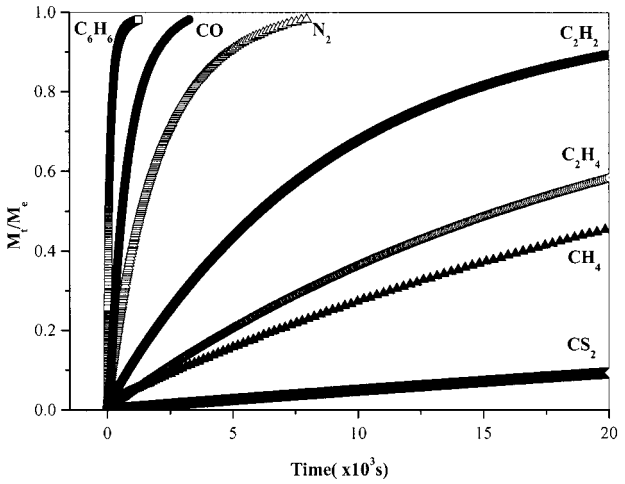

Figure 3. Variation of the gas uptake (M_t/M_e) with time for the adsorption of gases/vapors on CMS A: (a) ethylene (313 K, 50−60 kPa), (b) methane (343 K, 50−60 kPa), (c) benzene (313 K, 0−0.6 kPa), (d) nitrogen[8] (313 K, 20−30 kPa), (e) acetylene[8] (313 K, 20−30 kPa), (f) carbon monoxide[8] (313 K, 20−30 kPa), and (g) carbon disulfide[8] (343 K, 0−0.1 kPa).

−986 g mol^{-1}) and other gases studied previously,[6−8] but did not vary greatly with temperature.

The values for the isosteric heats of adsorption (Q_{st}) at zero surface coverage obtained from graphs of ln(A_0) versus 1/T are given in Table 2. The limiting values of Q_{st} at zero surface coverage for methane and ethylene were 23.8 ± 1.1 and 50.1 ± 1.5 kJ mol^{-1}, while the larger molecules chloroform, carbon tetrachloride, benzene, and pyridine were 44.7 ± 1.6, 44.1 ± 2.8, 41.8 ± 1.5, and 47.6 ± 0.9 kJ mol^{-1}, respectively.

Adsorption Kinetics. A number of kinetic models for diffusion of molecules into carbon molecular sieves have been used.[15−21] Linear driving force (LDF),[6−8,15] combined barrier resistance/Fickian diffusion,[6,8,16] and Fickian models[8,17] provide satisfactory descriptions, in most cases, of the adsorption kinetics of the various gases/vapors on CMS A depending on the adsorptive and experimental conditions.

The LDF model is described by the following equation:

$$M_t/M_e = 1 - \exp(-kt) \qquad (3)$$

where M_t is mass uptake at time t, M_e is mass uptake at equilibrium, and k is the kinetic rate constant. Graphs of M_t/M_e versus time for various pressure increments for ethylene, methane, benzene, carbon monoxide,[8] nitrogen,[8] acetylene,[8] and carbon disulfide[8] are shown in Figure 3. This illustrates the much faster adsorption of benzene compared with the other adsorptives. Graphs of ln($1-M_t/M_e$) against time for the uptake of ethylene (see Figure 4) and methane are linear (see Supporting Information), indicating that these gases follow an LDF mass-transfer-kinetic model[6−8] under the experimental conditions used. The adsorption kinetics can be compared in terms of the rate constants (k) for the LDF model, which are determined from the gradients of the kinetic plots (see Figure 4), or by fitting the adsorption uptake curves to eq 3. The kinetic data obtained from the LDF model for ethylene and methane adsorption on CMS A are given in Tables 3 and 4, respectively. It is apparent that while the rate constant increases with increasing relative pressure for both adsorptives for all the temperatures studied, it is particularly marked for ethylene adsorption. The adsorption kinetics for chloromethane followed an LDF model but were much slower than those of methane despite being of similar size. Therefore, only a single-adsorption isotherm, at 393 K, was measured for chloromethane. This showed that the rate constants increased with increasing surface coverage in a manner similar to the other adsorptives. The initial mass uptake versus time was almost linear for dichloromethane adsorption as shown in Figure 5. This is consistent with the adsorption kinetics for dichloromethane following an LDF model. The adsorption of dichloromethane at 343 K was so slow, with a predicted equilibrium time >180 days, that it was not practical to allow the system to reach equilibrium.

A combined barrier resistance/diffusion model[16] is based on the existence of a barrier resistance at the surface and subsequent diffusion in a spherical microporous system by Fick's law.[17]

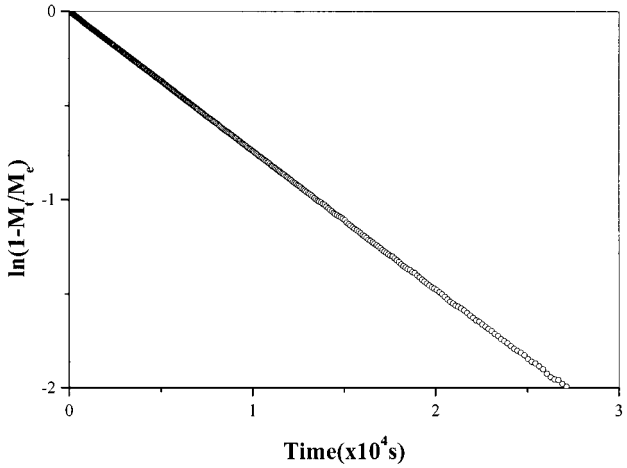

Figure 4. Variation of ln($1-M_t/M_e$) against time for the adsorption of ethylene (323 K, 70−80 kPa).

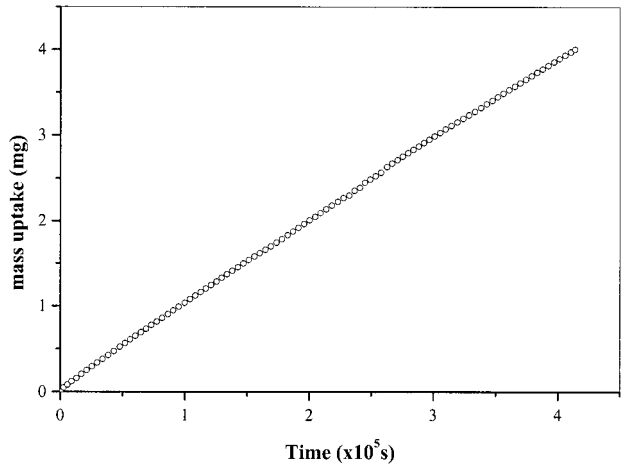

Figure 5. Graph of uptake (mmol g^{-1}) versus time for adsorption of dichloromethane on CMS A (358 K, 0−10 kPa) (only every 20th experimental data point plotted).

TABLE 3: Kinetic Data ($k/10^{-5}$ s^{-1}) for Ethylene Adsorption on CMS A[a]

	pressure increment/kPa					
temperature/K	0−50	50−60	60−70	70−80	80−90	90−100
303	1.020 ± 0.008	4.431 ± 0.020	5.191 ± 0.012	6.057 ± 0.018	7.124 ± 0.010	8.417 ± 0.042
313	1.291 ± 0.009	4.497 ± 0.008	5.949 ± 0.019	6.669 ± 0.009	8.775 ± 0.011	8.941 ± 0.031
323	1.695 ± 0.011	5.182 ± 0.009	6.653 ± 0.008	7.864 ± 0.008	8.996 ± 0.008	9.159 ± 0.009
333	2.668 ± 0.016	7.168 ± 0.011	8.568 ± 0.006	9.451 ± 0.016	10.830 ± 0.015	11.984 ± 0.016
343	3.409 ± 0.017	8.148 ± 0.007	11.046 ± 0.009	12.977 ± 0.015	14.510 ± 0.018	16.084 ± 0.035

[a] Temperature range 303−343 K; pressure range 0−100 kPa.

TABLE 4: Kinetic Data ($k/10^{-5}$ s^{-1}) for Methane Adsorption on CMS A[a]

	pressure increment/kPa					
temperature/K	0−50	50−60	60−70	70−80	80−90	90−100
338	2.192 ± 0.002	2.582 ± 0.008	2.735 ± 0.011	2.816 ± 0.015	3.154 ± 0.012	3.240 ± 0.014
343	2.639 ± 0.002	2.945 ± 0.009	3.108 ± 0.010	3.290 ± 0.018	3.585 ± 0.016	3.530 ± 0.014
348	3.672 ± 0.002	4.063 ± 0.020	4.245 ± 0.018	4.643 ± 0.020	4.938 ± 0.018	5.293 ± 0.013
353	4.584 ± 0.004	5.025 ± 0.023	5.217 ± 0.029	5.708 ± 0.021	6.245 ± 0.023	6.348 ± 0.030
358	5.995 ± 0.007	6.515 ± 0.029	6.964 ± 0.023	7.173 ± 0.042	8.005 ± 0.033	7.612 ± 0.052

[a] Temperature range 338−358 K; pressure range 0−100 kPa.

The relevant equations for isothermal diffusion into a spherical particle with this model are as follows:

$$\frac{\partial C}{\partial t} = D\left(\frac{\partial^2 C}{\partial r^2}\right) + \left(\frac{2}{r}\right)\left(\frac{\partial C}{\partial r}\right) \tag{4}$$

where D is the crystallite diffusivity (cm^2 s^{-1}), C is the sorbate concentration in the crystallite (mmol cm^{-3}), r is the radial coordinate, and t is the time.

$$D\frac{\partial C(r_c,t)}{\partial r} = k_b\{C^*(t) - C(r,t)\} \tag{5}$$

where D is the crystallite diffusivity (cm^2 s^{-1}), k_b is the barrier resistance (cm s^{-1}), r_c is the radius of the particle (cm), r is the radial coordinate, t is the time, C is the sorbate concentration in the crystallite (mmol cm^{-3}), and C^* the surface concentration in equilibrium with the gas phase (mmol cm^{-3}). The parameters derived from the model are k_b, the barrier resistance constant, and k_d which is equal to D/r_c^2. A full description of the method of solving the equation has been described previously.[6,8] A comparison of the calculated profile from the combined barrier resistance/diffusion model with the experimental profile for a typical pressure increments for chloroform adsorption on CMS A is shown in Figure 6. Similar typical experimental and calculated profiles for carbon tetrachloride, benzene, and pyridine are provided in Supporting Information. It is apparent that the combined barrier resistance/Fickian model provides a good description of the adsorption kinetics for chloroform, carbon tetrachloride, and pyridine while benzene adsorption follows an LDF model. The kinetic parameters derived from these models confirm the fast adsorption kinetics compared with methane, ethylene, acetylene,[8] argon,[6] etc.

Fick's law for isothermal diffusion into a homogeneous sphere is given by eq 3. The solution to this equation is

$$\frac{M_t}{M_e} = 1 - \frac{6}{\pi^2}\sum_{n=1}^{\infty}\left(\frac{1}{n^2}\right)\exp\left(\frac{-Dn^2\pi^2 t}{r^2}\right) \tag{6}$$

where M_t is mass uptake at time t, M_e is mass uptake at equilibrium, D is diffusivity, and r is radius of the particle. The above series converges very rapidly and a graph of $\ln(1 - M_t/M_e)$ versus time is close to linearity in the uptake region M_t/M_e >0.6. Therefore, the graph only differs from the LDF model in the initial uptake region where M_t/M_e <0.6. A Fickian diffusion model fitted the adsorption kinetic data for pyridine adsorption on CMS A over the p/p^0 range 1.2−1.4 kPa at 303 K and the fit for a typical pressure increment is shown in Figure 7.

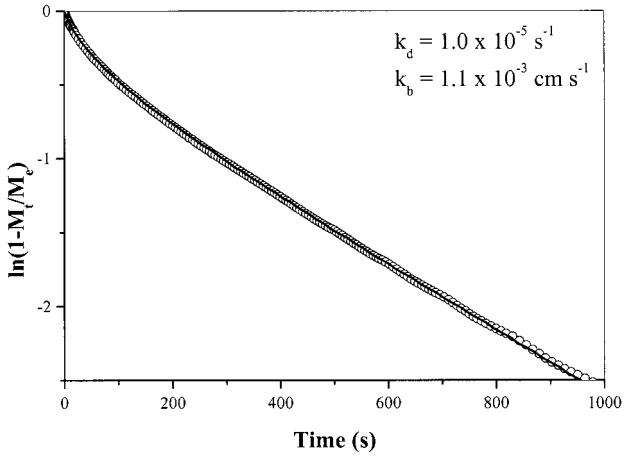

Figure 6. Comparison of the $\ln(1-M_t/M_e)$ versus time graph for adsorption of chloroform on CMS A (273 K, 100−200 Pa) (only every fifth experimental data point plotted; (−) combined barrier resistance/diffusion model).

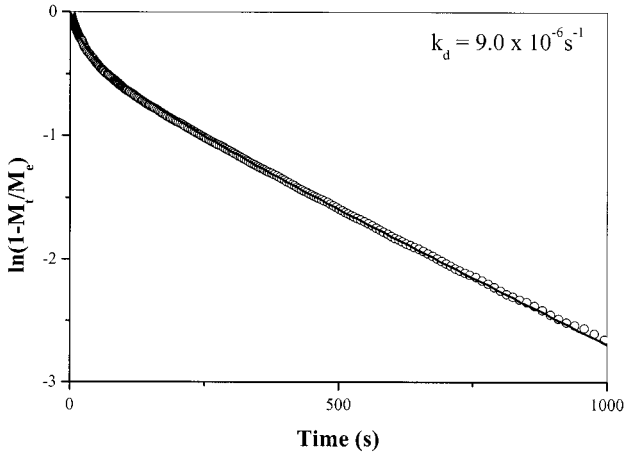

Figure 7. Comparison of the $\ln(1-M_t/M_e)$ versus time graph for pyridine (303 K, 1.2−1.4 kPa) uptake on CMS A (only every second experimental data point plotted; (−) Fickian diffusion model).

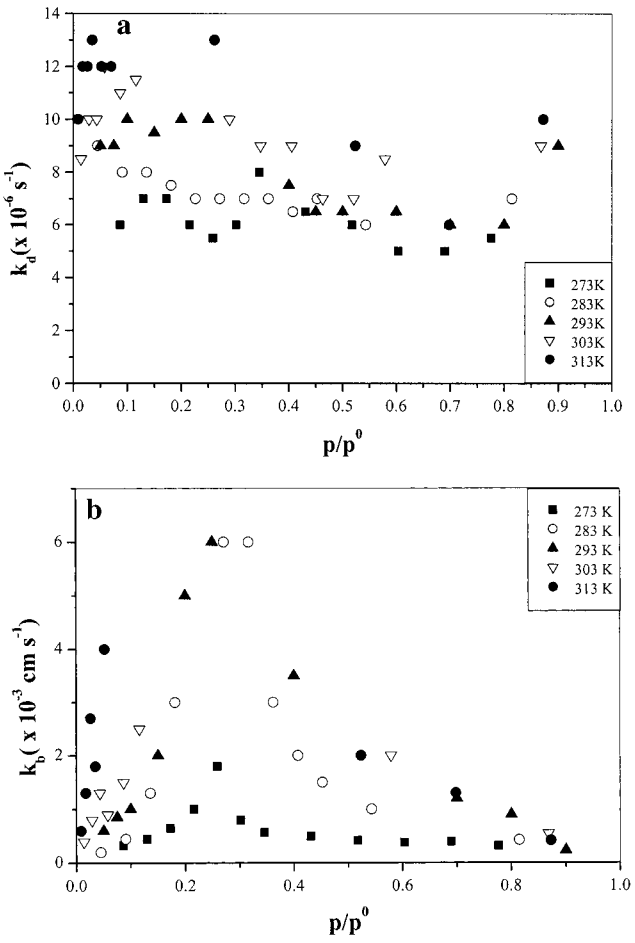

Figure 8. Kinetic data for pyridine adsorption on CMS A obtained using the combined barrier resistance/diffusion model: Temperature range 273−313 K (273 K (■), 283 K (○), 293 K (▲), 303 K (▽), 313 K (●)): (a) k_d and (b) k_b.

The kinetic models described fitted the adsorption kinetics for carbon tetrachloride and chloroform at low pressure but not over most of the pressure range. In the case of pyridine adsorption, at low pressures the adsorption kinetics followed a combined barrier resistance/Fickian diffusion model, which changed to a Fickian model with increasing pressure and back to the combined barrier resistance/diffusion model. The barrier resistance (k_b) and diffusion (k_d) constants obtained from the combined barrier resistance/Fickian model for pyridine adsorption are shown in Figures 8a and 8b. It is apparent that for a given temperature the value of k_d does not change greatly, whereas k_b reaches a maximum at $p/p^0 \sim 0.25$, which corresponds to 0.6 mmol g^{-1} uptake i.e., micropore filling. At this relative pressure, a Fickian-diffusion mechanism is followed at higher adsorption temperatures, when diffusion through the barrier is fast compared with diffusion along the pores.

Discussion

Adsorption Isotherms. The adsorption characteristics of a range of adsorptives on microporous materials can be compared using the Dubinin−Radushkevich (D−R) equation,[22] which is as follows:

$$\log n = \log n_0 - D \log^2(p^0/p) \qquad (7)$$

where n is the amount adsorbed, n_0 the amount adsorbed corresponding to the micropore volume, p the pressure, p^0 the saturated vapor pressure, and D is a constant related to the

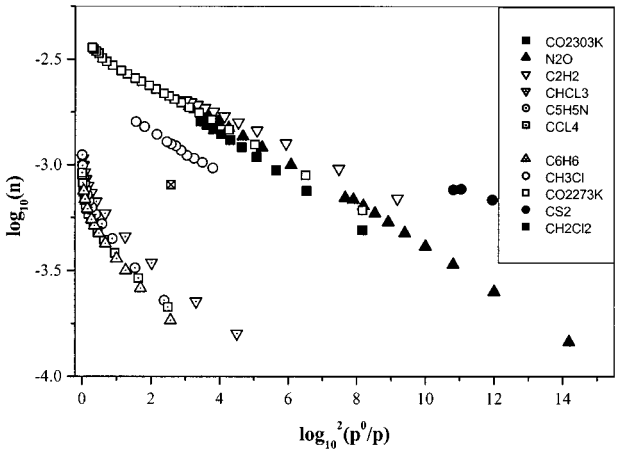

Figure 9. Dubinin−Radushkevich graphs for adsorption of gases and vapors on CMS A at 303 K and chloromethane at 393 K (data for N_2O, CO_2, C_2H_2, and CS_2 from ref 8).

microporous structure of the adsorbent. The D−R graphs for the data, where the adsorptive vapors are below the critical temperatures, are compared with those of carbon dioxide, nitrous oxide, and acetylene at 303 K in Figure 9. Adsorption data for chloromethane (critical temperature 416.3 K) on CMS A at 393 K and carbon disulfide (340−355 K) are also shown in Figure 9. The adsorption kinetics for carbon disulfide adsorption were very slow at all the temperatures studied.[8] Although uptakes were greater than 90% of the equilibrium values, it was necessary to estimate the equilibrium uptakes from the weight-versus-time profiles using the LDF model. Therefore, these data are of lower accuracy than if equilibrium had been determined experimentally. However, the data shows unequivocally that carbon disulfide is not excluded to a significant extent from the microporous structure. Chloromethane is, at most, excluded from a small part of the microporous structure. This adsorptive can be regarded as close to the upper-size limit of molecules which can pass through the selective porosity before complete exclusion of the adsorptive by the selective porous structure occurs. However, the D−R graphs for chloroform, carbon tetrachloride, benzene, and pyridine adsorption on CMS A are very similar to each other with a marked upward curvature at high relative pressures but the amount adsorbed at a given relative pressure is much lower than for carbon dioxide, nitrous oxide, acetylene, carbon disulfide, and chloromethane at the same relative pressure. The total pore volumes obtained for the four adsorptives were identical (∼0.10 cm^3 g^{-1}) within experimental error. This indicates that the larger adsorptives are excluded by the selective porosity from the same microporous structure.

When considering adsorption characteristics, in the case of an adsorbent with slit shaped pores, the minimum size of the molecule in one dimension (MIN-1) is critical. In the case of an adsorbent with cylindrical pores with spherical cross-section, the minimum sizes of the molecule in two dimensions (MIN-1 × MIN-2) need to considered.[23−25] Molecular diameters have been calculated by a wide variety of methods, for example, from van der Waals radii, molecular models etc.[26] However, estimates of molecular diameter values differ considerably depending on the method used, for example, for nitrogen the values were in the range 300−433 pm (average 335 pm).[26] The minimum dimensions of the suite of molecules used in this study have been calculated using Zero Integral Neglect of Differential Overlap (ZINDO) methods and these data are given in Table 5.[23−25] These differences in the size and structure of the adsorptives need to be considered in relation to exclusion of

TABLE 5: Comparison of the Molecular Dimensions (pm) Obtained from ZINDO Calculations for the Probe Molecules[23−25] Used in This and Previous Related Studies[6−8]

adsorptive	dimensions/pm		
	Spherical		
argon[a]	351	363	
	Linear		
oxygen[b]	293.0	298.5	405.2
nitrogen[b]	299.1	305.4	404.6
carbon monoxide[b]	328.0	333.9	418.2
carbon dioxide[b]	318.9	333.9	536.1
nitrous oxide[c]	303	304	532
acetylene[c]	332	334	570
carbon disulfide[b]	337.6	353.5	665.5
	Planar		
ethylene[c]	328	418	484
benzene[b]	327.7	662.8	733.7
pyridine[b]	333.9	647.5	664.8
	Tetrahedral		
methane[b]	382.9	394.2	410.1
chloromethane[c]	396	413	518
dichloromethane[c]	414	457	626
chloroform[b]	461.3	571.3	618.1
carbon tetrachloride[b]	572.3	574.8	620.7

[a] Data from ref 24. [b] Data from ref 23. [c] C. E. Webster and M. Zerner (Private Communication, ref 25).

the adsorptives from part of the porous structure of CMS A. In particular, benzene and pyridine have the two minimum dimensions (MIN-1 and MIN-2) of 327.7 × 662.8 and 333.9 × 647.5 pm, respectively. Both adsorptives are excluded to similar extents to chloroform and carbon tetrachloride, which have minimum dimensions of 461.3 × 571.3 and 572.3 × 574.8 pm, respectively. Carbon dioxide (318.9 × 333.9 pm) and carbon disulfide (337.6 × 353.5 pm) are adsorbed on CMS A without any significant exclusion of the adsorptive from the microporous structure. Therefore, it is reasonable to conclude that the intermediate minimum dimension (MIN-2), being much larger than MIN-1 for benzene and pyridine, causes exclusion from a large part of the microporous structure. Therefore, the adsorption isotherms suggest that the selective porosity behaves as though it has approximately spherical symmetry and there is no evidence for marked-slit shaped character. This is rather surprising bearing in mind that microporous carbons are comprised of graphene layers.

The size-exclusion characteristics of the selective porosity can be inferred from graphs of either the amounts adsorbed corresponding to the micropore volumes (see Figure 10) obtained from the linear parts of the D−R graphs or amounts adsorbed at a specific p/p^0 versus the larger of the two minimum dimensions of the adsorptives (see Figure 11). The conversion of amounts adsorbed to micropore volumes is not straightforward when adsorption takes place close to the critical temperatures of the adsorptives because the true densities of the adsorbed phase may be higher than the liquid density at the adsorption temperature. An example of this is the evaluation of the micropore volume from chloromethane (critical temperature 416.3 K) adsorption at 391 K. The uptake corresponding to the micropore volume was 2.25 ± 0.04 mmol g^{-1}, while the limited information available for the density of liquid chloromethane shows that it varies from 0.9963 g cm^{-3} at 249 K to 0.849 g cm^{-3} at 327.6 K.[27] The variation in liquid density with temperature makes it difficult to establish unequivocally the density of the adsorbed phase, which may be influenced by adsorbate/adsorbent interactions and molecular packing effects. The kinetic studies show that for dichloromethane (molecular

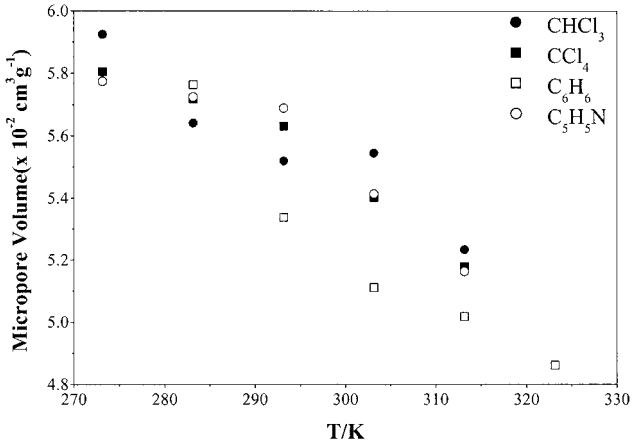

Figure 10. Graph of micropore volume versus adsorption temperature for benzene (□), pyridine (○), chloroform (●) and carbon tetrachloride (■).

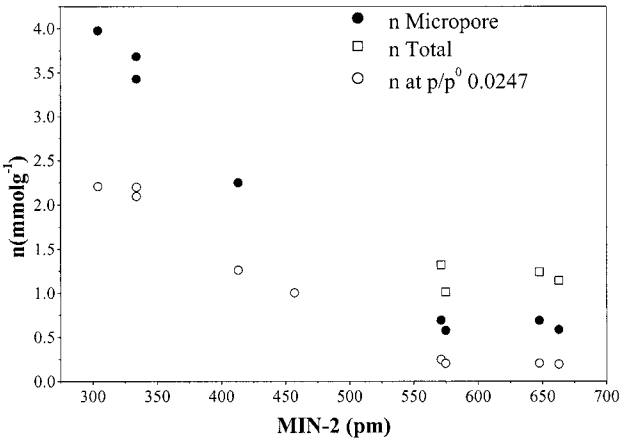

Figure 11. Graph of adsorption uptakes (mmol g^{-1}), corresponding to micropore and total pore volumes and amount adsorbed at p/p^0 ~0.0247 for various gases and vapors versus adsorptive dimension MIN-2 (data for N_2O, CO_2 and C_2H_2 from ref 8).

dimensions 414 × 457 pm) the adsorption kinetics were very slow. An estimate of dichloromethane adsorption uptake at equilibrium was calculated from the kinetic data using the LDF model. The uptake after 4 × 10^5 s was ~0.09 mmol g^{-1} with an estimated equilibrium uptake of 0.422 mmol g^{-1} at p/p^0 = 0.0247 and equilibrium time of over 180 days for 99% uptake. In this case, the liquid density can be used to calculate the volume of adsorbate. Although there is a relatively high uncertainty in the estimated value compared with experimentally determined values, the graph of amount adsorbed at p/p^0 = 0.0247 versus the intermediate adsorptive dimension MIN-2 (see Figure 11) is consistent with dichloromethane (414 × 457 pm) being accessible to part (~50%) of the selective microporous structure. The graphs of micropore volume obtained for adsorption at 303 K and chloromethane at 393 K versus MIN-2 were similar in shape but the data for dichloromethane were not available (see Figure 11). The data for carbon disulfide adsorption are unequivocal in that there is no exclusion for adsorptives of sizes up to ~350 pm. The adsorption data for chloroform, carbon tetrachloride, benzene, and pyridine show that there is exclusion from the selective part of the porous structure for MIN-2 ~570 pm. Furthermore, the selective microporosity may be assessed from the difference between the micropore volume for carbon dioxide adsorption and the micropore volumes for the excluded adsorptives (chloroform, carbon tetrachloride, benzene, and pyridine). The micropore

volume calculated from the linear portion (24 data points) of the carbon dioxide adsorption isotherm (0−900 kPa) at 273 K was 0.1587 ± 0.0010 $cm^3\ g^{-1}$ based on a density of adsorbed carbon dioxide of 1.023 g cm^{-3}.[28] The meso/macropore volume can be estimated from the differences between the total and micropore volumes for the excluded adsorptives. Since a small variation in nonselective micropore volume was observed with temperature (see Figure 10), the average value (0.059 $cm^3\ g^{-1}$) at 273 K (same temperature as carbon dioxide isotherm) was used. These data show that the carbon molecular sieve studied has ∼50% selective microporosity, ∼30% nonselective microporosity, and ∼20% meso/macroporosity. This method provides a detailed evaluation of the adsorption characteristics of the carbon molecular sieve.

Virial Parameters. Previous comparisons of the virial parameters of adsorptives with results obtained for cases where the carbon was nonselective in terms of kinetics showed that the values were quite similar to those obtained for adsorption on the selective CMS.[6−8,14,29,30] The values of A_1 were not strongly temperature dependent. It is apparent that the virial parameters obtained in this study for the adsorption of chloroform, carbon tetrachloride, benzene, and pyridine are much higher −3000 to −5000 g mol^{-1}. Previous studies of the adsorption of CF_3Cl on microporous carbons gave values of −960 to −1830 g mol^{-1} over the temperature range 273.2 to 293.2 K.[29] However, these data were obtained from the extrapolation of data for adsorption uptakes of >0.7 mmol g^{-1}, whereas the data in Figure 2 show a change of gradient at ∼0.6 mmol g^{-1}. Therefore, the absence of low surface coverage data in previous studies is probably the reason for the difference. The values of the virial parameter A_1 obtained for adsorption of methane on a carbosieve were −540 to −650 g mol^{-1} for the temperature range 273.2−312 K. These values are much closer to the values reported in this work and reported in our previous studies of the adsorption of nitrogen, oxygen, carbon monoxide, argon etc. on CMS A.[6,8]

Isosteric Enthalpies of Adsorption. Table 2 shows a comparison of the isosteric enthalpies of adsorption with literature values for adsorption of various gases/vapors on a range of microporous and molecular sieve carbons at low surface coverage. The values reported in this paper are similar to those obtained previously for microporous carbons and carbon molecular sieves.[6−8,29−34] In comparison, the isosteric heats of adsorption for oxygen, nitrogen, argon, carbon monoxide, carbon dioxide,[5] and ethylene[32,33] on the graphite basal plane were approximately half the corresponding values for adsorption on microporous materials.[6−8,14,30,34] The difference was attributed to the overlap of the potential energy fields of the pore walls in the microporous materials.[8]

The virial parameters A_0 and A_1 for the adsorption gases not excluded by the selective porosity in CMS A are plotted against the isosteric enthalpy of adsorption (Q_{st}) at zero surface coverage in Figures 12a and 12b. It is apparent that A_0 increases while A_1 becomes more negative with increasing Q_{st}. A_0 and A_1 also correlate well with each other, which makes it difficult to separate adsorbate/adsorbent and adsorbate/adsorbate interactions. However, a higher Q_{st} is consistent with a larger value of the Henry's Law constant (K_H) where $K_H = \exp(A_0)$.

Adsorption Kinetics. Rao et al. developed a model[4,5] for the interaction potential of diffusing species in pores based on the previous model of Steele[35] for the interaction of gases with carbon surfaces, and concluded that two processes are involved in the adsorption dynamics: (a) diffusion along the pores; and (b) diffusion through the barrier at the pore entrance. An LDF model is followed when the latter is the rate-determining step. When diffusion along the pores becomes a significant factor, a model based on a combined barrier resistance/diffusion mechanism provides a good description of the adsorption kinetics. If the barrier at the pore entrance is low then diffusion along the pores may control the adsorption kinetics and a Fickian diffusion model is obeyed.

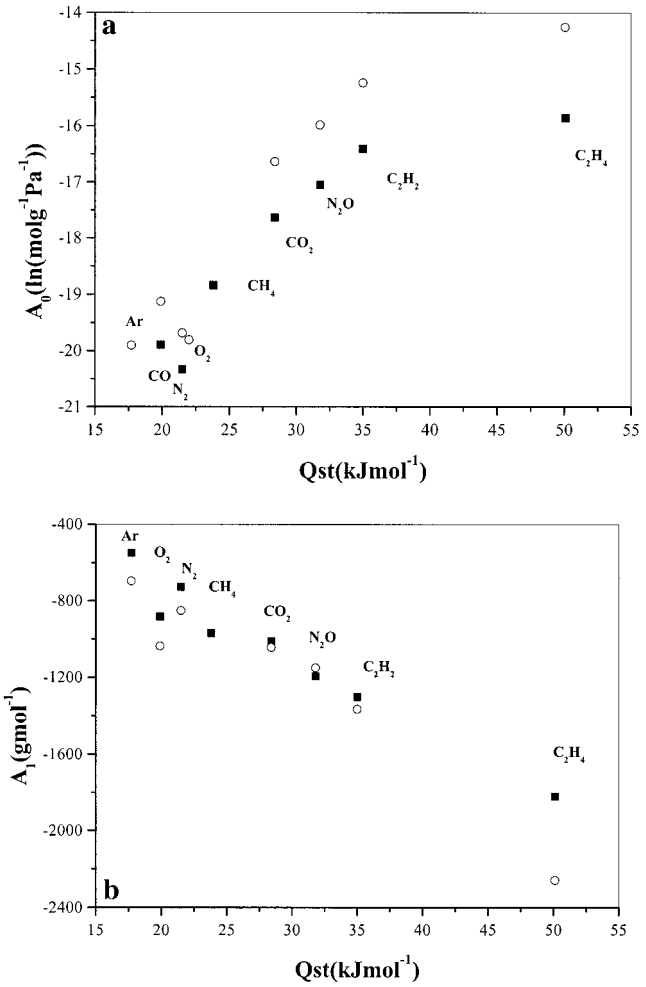

Figure 12. Graph of virial parameters versus isosteric heat of adsorption (Q_{st}) for the adsorptives not excluded completely by the selective porosity (a) A_0 (○, 313 K; ■, 343 K) and (b) A_1 (○, 313 K; ■, 343 K).

The adsorption kinetics for ethylene and methane on CMS A followed an LDF model similar to the results obtained[6,8] for oxygen nitrogen, carbon monoxide, argon, acetylene, and krypton, which are not excluded by the selective porosity. In contrast, carbon dioxide (not excluded by the selective porosity) adsorption on CMS A over the temperature range 303−343 K, followed an LDF model at low pressures and temperatures which changed to a combined barrier resistance/Fickian diffusion model[16] and Fickian[17] models with increasing temperature and pressure. This showed that a single adsorptive/adsorbent system can exhibit a full range of kinetic behavior from LDF to Fickian diffusion depending on the experimental conditions used.

Chloroform, carbon tetrachloride, benzene, and pyridine are partly excluded from the porous structure of CMS A by the selective porosity. Therefore, the adsorption kinetic characteristics cannot be compared directly with the other adsorptives and these four adsorptives must be considered separately. The adsorption kinetics of chloroform (see Figure 6), carbon tetrachloride, and pyridine follow a combined barrier resistance/

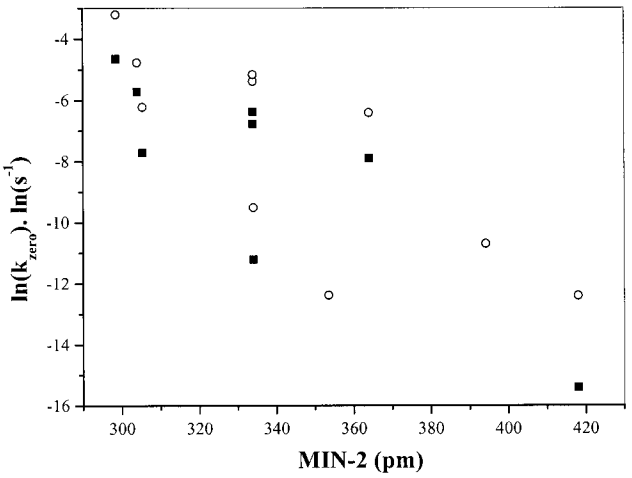

Figure 13. Variation of ln(k) at zero surface coverage versus adsorptive dimensions MIN-2 (■, 313 K; ○, 343 K).

diffusion model at low pressure, which gives parameters for the barrier (k_b) and diffusion (k_d) components of the model (see Supporting Information). Benzene adsorption followed an LDF model at low pressure, which changed to the combined barrier resistance/diffusion model with increasing pressure. Pyridine adsorption showed clear trends changing from a combined barrier resistance/Fickian diffusion model at low relative pressures to a Fickian diffusion model and back again at higher relative pressures. This change in adsorption kinetic model is associated with filling of the nonselective microporosity. The modeling of the adsorption kinetics for other adsorptives showed that the kinetics usually obeyed a combined barrier resistance model at low relative pressure but at higher relative pressures the kinetics did not follow this or Fickian and LDF models. The modeling of the kinetics of adsorption of carbon dioxide on CMS A[8] using the combined barrier resistance/diffusion model[16] showed that k_d decreased slightly with increasing pressure while k_b increases markedly with increasing pressure. Large changes in k_b were also observed for pyridine adsorption but with little or no change in k_d (see Figures 8a and 8b).

Comparison of Adsorption Kinetics at Zero Surface Coverage. Comparisons of adsorption kinetics need to be carried out at the same surface coverage because the kinetic rate constants vary with surface coverage. Therefore, the rate constants at zero surface coverage have been used. The isotherm results indicate that exclusion of molecules occurs and that the selective porosity behaves as though it has approximately spherical characteristics, which means that two dimensions (MIN-1 and MIN-2) need to be considered with MIN-2 being the most critical size parameter. The variation of adsorption rate constant for the full range of gases/vapors on CMS A at 313 and 343 K with adsorptive dimension MIN-2 are shown in Figure 13. Where the experimental values are not available, the values have been calculated using the data obtained from the Arrhenius equation over a different temperature range. It is apparent that there is a general decrease in rate constant with increasing adsorptive size, although there is some scatter in the data resulting from contributions from other factors. This is evident from comparison of the minimum molecular dimensions and adsorption rate constants for nitrogen (299.1 × 305.4 × 404.6 pm) and carbon monoxide (328.0 × 333.9 × 418.2 pm) that the latter is larger while the adsorption kinetics are faster.[8] Comparison of the molecular cross-section dimensions of carbon dioxide (318.9 × 333.9 × 536.1 pm) and acetylene (332 × 334 × 570 pm) show that the adsorption rate constants of the latter are much slower than the former despite the two molecules having very similar molecular cross-section dimensions. The fast rates of nitrous oxide adsorption are consistent with the relatively small cross-sectional dimensions (303 × 304 × 532 pm) but these dimensions are very similar to those of nitrogen, which has much smaller rate constants. The relatively fast adsorption kinetics for N_2O and CO_2 compared with argon and N_2 indicates that the length of a molecule is not a major factor in determining the kinetics.

Comparisons of adsorption kinetics with adsorptive dimensions are difficult because there is the possibility of partial exclusion of the adsorptive from the porous structure making direct comparisons invalid. It is apparent from the comparison of the data in Figure 13 and the adsorption kinetics that the minimum dimensions of the molecules do not always provide a good guide to the adsorption kinetics but there is a general trend of decreasing rate constant with increasing minimum cross-section size.

When the rate of adsorption is fast and the isosteric heat of adsorption relatively high, as is the case for carbon dioxide and nitrous oxide and also carbon tetrachloride, chloroform, benzene, and pyridine, diffusion along the pores becomes a rate-determining factor and a combined barrier resistance/Fickian diffusion model is observed. In some circumstances, diffusion along the pores becomes the rate-determining step.

The adsorption kinetics of both methane and chloromethane follow an LDF model indicating that diffusion through a barrier is the rate-determining step. However, the rate of adsorption of chloromethane is much slower (factor ~30) than methane at low surface coverage and required a temperature of 393 K to obtain acceptable kinetics in order to obtain an isotherm. A comparison of the rates of chloromethane (393 K) and methane (343 K) adsorption as a function of surface coverage are given in Supporting Information. Despite a 50 K difference in temperature and a higher surface coverage, it is apparent that the adsorption of chloromethane is comparatively slow. Clearly, this difference in adsorption kinetic rates can be ascribed to size factors but chloromethane is partly excluded by the selective porosity. Since diffusion through the barrier is the rate-determining step, the electronic interaction between the chlorine and the selective porosity is possibly the factor since surface diffusion along the pores is not the rate-determining step. This is supported by the observation of very slow rates of adsorption for carbon disulfide (337.6 × 353.5 × 665.5 pm). It is proposed that the more polarizable chlorine and sulfur have stronger interactions with the selective porosity than the first row elements. This illustrates the complex nature of the factors, which influence adsorption kinetics.

Comparison of Activation Energies. Adsorption kinetics for gases and vapors ranging from hydrophilic to hydrophobic on active carbon exhibit a compensation effect where the activation energy (E_a) correlates with ln(preexponential factor) (ln(A)).[36−38] This compensation effect has also been observed for the adsorption of methanol and ethanol on a porous metal organic framework material $Ni_2(4,4'\text{-bipyridine})_3(NO_3)_4$.[39] This suggests that the effect is general for adsorption on porous materials. The variation in activation energy and ln(preexponential factor) with surface coverage is weak for the adsorptives used in this study and only apparent for adsorptives where the surface coverage is high. To compare the activation energies for the various adsorptives, the activation energies at zero surface coverage were calculated by extrapolation of the kinetic data as a function of surface coverage. Previous studies[6,8] of a wide range of adsorption of spherical and linear gases and vapors on

TABLE 6: Activation Energies and Preexponential Factors for Adsorption on the Carbon Molecular Sieve CMS A at Specific Surface Coverages

	CH_4				
	surface coverage (mmol g^{-1})				
	0	0.1	0.2	0.25	0.3
E_a (kJ mol^{-1})	53.6 ± 2.2	54.6 ± 2.4	53.0 ± 2.8	54.3 ± 3.4	55.6 ± 3.7
ln(*A*)	8.11 ± 0.77	8.6 ± 0.8	8.2 ± 1.0	8.6 ± 1.2	9.2 ± 1.3
	C_2H_4				
	surface coverage (mmol g^{-1})				
	0[a]	0.6	0.8	1.0	1.2
E_a (kJ mol^{-1})	76 ± 15	67.5 ± 2.6	64.7 ± 1.8	65.0 ± 2.8	65.6 ± 1.5
ln(*A*)	14.5 ± 5.5	12.9 ± 1.0	12.5 ± 0.7	13.2 ± 1.0	14.2 ± 0.6

[a] Calculated by extrapolation of the ln(*k*) versus *n*/mmol g^{-1} graphs (excluding the kinetics of the first isotherm point) to zero surface coverage.

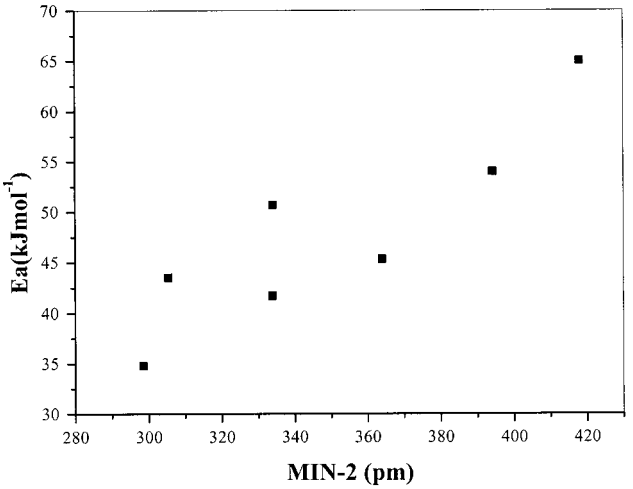

Figure 14. Graph of activation energy versus adsorptive dimension MIN-2 for the adsorptives not excluded completely by the selective porosity in CMS A.

CMS A have shown that graphs of ln(*k*) versus amount adsorbed are linear. The large initial pressure steps (0−50 kPa) for ethylene adsorption were used to obtain acceptable equilibrium times for the isotherm studies, but these gave large uptakes and, therefore, the variation in adsorption kinetics over the adsorption uptake for these steps was relatively large. Therefore, these points were not used in the graphs to obtain the values of ln(*k*) at zero surface coverage. Extrapolation of the data for ethylene adsorption is liable to larger inaccuracies than the other data because of the relatively long extrapolation. The values of E_a and ln(*A*) at zero surface coverage were 76 ± 15 kJ mol^{-1} and 14.5 ± 5.5 ln(s^{-1}), respectively. These values are not significantly different from the values given in Table 6, which were obtained at higher surface coverage. The activation energies for methane and ethylene in this study and the data reported previously[6,8] for the noble gases and linear adsorptives, which also follow the LDF model where diffusion through the barrier is the rate-determining step, are plotted against MIN-2, calculated using the ZINDO method,[23−25] in Figure 14. The average of the E_a values obtained at higher surface coverage for ethylene adsorption were used in the graph because of the high standard deviation in the value for zero surface coverage. It is evident that there is an increase in activation energy with increasing adsorptive dimension MIN-2, which is consistent with diffusion through the barrier being the rate-determining step.

Conclusions

The CMS used in this study is used for air separation but it also adsorbed a wide range of adsorptives of varying sizes. The adsorption kinetics of various probe molecules are a complex function of the size, shape, and electronic structure of the adsorptive. The following factors need to be considered (1) exclusion by the selective porosity, (2) diffusion through the selective porosity, (3) diffusion along the pores, and (4) adsorbate/adsorbent interactions. The micropore and total pore volumes obtained from the adsorption isotherms for planar molecules benzene and pyridine (minimum dimensions of ∼330 × 650 pm), and chloroform (461.3 × 571.3 pm) and carbon tetrachloride (572.3 × 574.8 pm), clearly show that all four adsorptives are excluded from the bulk of the microporous structure to virtually the same extent. In contrast, linear molecules, for example, carbon disulfide (∼337.6 × 353.5 pm) and acetylene (332 × 334 pm) are adsorbed without significant exclusion. This indicates that the intermediate of the three dimensions is important in excluding the adsorptive from the porous structure and hence that the selective porosity behaves as though it has approximately spherical structural characteristics. It was apparent that there was a sharp cut off in the exclusion of molecules in the range ∼400−500 pm with partial exclusion giving extremely slow adsorption kinetics.

The micropore volumes for the probe molecules, which are not excluded (carbon dioxide etc.) and those that are excluded (benzene, carbon tetrachloride etc.) by the selective porosity gave the total (selective + nonselective) and nonselective micropore volumes, which allowed the selective micropore volume to be determined from the difference between these values. The meso/macro pore volumes were determined from the difference between the total pore and nonselective micropore volumes obtained using the probe molecules excluded by the selective porosity. This allowed the porous structure to be characterized as ∼50% selective microporosity, 30% nonselective porosity and 20% meso/macroporosity. This method has general application in the detailed characterization of heterogeneous molecular sieves.

The adsorption kinetics for the wide range of gases used usually followed an LDF model but deviations occurred for chloroform, carbon tetrachloride, benzene, and pyridine where partial exclusion from the porous structure occurred. Similar deviations also occurred for carbon dioxide and nitrous oxide adsorption where there was no evidence for exclusion from the porous structure. The model for adsorption kinetics varied from LDF through combined barrier resistance/diffusion model to Fickian diffusion for carbon dioxide adsorption depending on the experimental conditions. Comparison of adsorption kinetic parameters for the probe molecules shows that simplistic comparisons of size do not always produce the correct order whereas adsorptive dimensions are invaluable in determining the size exclusion characteristics of the adsorbent. The adsorption kinetic data show that the rate constants decrease by ∼4 orders of magnitude for increasing size from ∼290 to 420 pm. Even within this, there are differences which can only be explained by differences in specific adsorbate/adsorbent interactions with the selective porosity. These interactions play a significant role in determining the adsorption kinetics. The relative rates of diffusion of the adsorbate through the selective porosity are a function of the molecular size, shape, and electronic interaction while diffusion along the pores is a function of surface diffusion, which is related to the isosteric heat of adsorption.

Acknowledgment. The authors would like to thank the EPSRC for supporting this project under grant GR/J86421 and a studentship for CR. The authors would like to thank Dr. C.E. Webster of Texas A&M University and the late Dr. M.C. Zerner of Florida State University for providing additional calculations of the adsorptive dimensions for ethylene, nitrous oxide, acetylene, chloromethane, and dichloromethane.

Supporting Information Available: Adsorption isotherm and kinetic data are available free of charge via the Internet at http://pubs.acs.org.

References and Notes

(1) Armor, J. N. In *Separation Technology;* Vansat, E. F., Ed.; Elsevier Science B. V.: Amsterdam, 1994, p 163.
(2) Verma, S. K. *Carbon* **1991**, *29*, 793.
(3) Chagger, H. K.; Ndaji, F. E.; Sykes, M. L.; Thomas, K. M. *Carbon* **1995**, *33*, 1405.
(4) Rao, M. B.; Jenkins, R. G.; Steele, W. A. *Ext. Abstr. 17th Biennial Conf. Carbon*; University of Kentucky, Lexington; American Carbon Society: 1985; p 114.
(5) Rao, M. B.; Jenkins, R. G.; Steele, W. A. *Langmuir* **1985**, *1*, 137.
(6) Reid, C. R.; O'Koye, I. P.; Thomas, K. M. *Langmuir* **1998**, *14*, 2415.
(7) O'Koye, I. P.; Benham, M.; Thomas, K. M. *Langmuir* **1997**, *13*, 4054.
(8) Reid, C. R.; Thomas, K.M. *Langmuir* **1999**, *15*, 3206.
(9) Chihara, K.; Suzuki, M. *Carbon* **1979**, *17*, 339.
(10) Benham, M.; Ross, D. K. *Z. Phys. Chem.* **1989**, *163*, 25.
(11) CRC *Handbook of Chemistry and Physics*, 74th ed.; CRC Press: Boca Raton, FL, 1993.
(12) *Lange's Handbook of Chemistry*, 15th ed.; McGraw-Hill: New York, 1999.
(13) Gregg, S. J.; Sing, K. S. W. *Adsorption, Surface Area and Porosity*, 2nd ed.; Academic Press: New York, 1982.
(14) Cole, J. H.; Everett, D. H.; Marshall, C. T.; Paniego, A. R.; Powl, J. C.; Rodriguez-Reinoso, F. *J. Chem. Soc., Faraday Trans. 1* **1974**, *70*, 2154.
(15) Braymer, T. A.; Coe, C. G.; Farris, T. S.; Gaffney, T. R.; Schork, J. M.; Armor, J. N. *Carbon* **1994**, *32*, 445.
(16) Loughlin, K. F.; Hassan, M. M.; Fatehi, A. I.; Zahur, M. *Gas Sep. Purif.* **1993**, *7*, 264.
(17) Crank, J. *The Mathematics of Diffusion*, 2nd ed.; Clarendon Press: Oxford, 1975.
(18) LaCava, A. I.; Dominguez, J.; Cardenas, J. *Adsorpt. Sci. Technol.* **1988**, *158*, 323.
(19) LaCava, A. I.; Koss, V. A.; Wickens, D. *Gas Sep. Purif.* **1989**, *3*, 180.
(20) Dominguez, J. A.; Psaras, D.; LaCava, A. I.; A. I. Ch. E. *Symp. Ser.* **1988**, *84*, 73.
(21) Rutherford, S. W.; Do, D. D. *Langmuir* **2000**, *16*, 7245.
(22) Dubinin, M. M. In *Characterisation of Porous Solids;* Sing, K. S. W., Ed; Society of Chemical Industries, 1979; Vol. 1, pp 1−11.
(23) Webster, C. E.; Drago, R. S.; Zerner, M. C. *J Am. Chem. Soc.* **1998**, *120*, 5509.
(24) Webster, C. E.; Cottone, A.; Drago, R. S. *J. Am. Chem. Soc.* **1999**, *121*, 12127.
(25) Webster, C. E.; Zerner, M. C. (private communication: calculated by the methods used in ref 23).
(26) Ainscough, A. N.; Dollimore, D. *Langmuir* **1987**, *3*, 708.
(27) *Handbook of Compressed Gases*, 3rd ed.; Van Nostrand Reinhold: New York, 1990.
(28) Rodriguez-Reinoso, F.; Linares-Solano, A. In *Chemistry and Physics of Carbon*; Thrower, P. L., Ed.; Marcel Dekker: New York, Vol. 21, 1989, p 1.
(29) Carrot, P. J. M.; Sing, K. S. W *Adsorpt. Sci. Technol.* **1989**, *6*, 136.
(30) Floess, J. K.; Kim, H. H.; Edens, G.; Oleksy, S. A.; Kwak, J. *Carbon* **1992**, *30*, 1025.
(31) Avgul, N. N.; Kiselev, A. V. In *Chemistry and Physics of Carbon*; Walker, P. L., Jr., Ed.; Marcel Dekker: New York, Vol. 6, 1970, p 1.
(32) Kalashnikova, E. V.; Kiselev, A. V.; Petrova, R. S.; Shcherbakova, K. D. *Chromatographia* **1971**, *4*, 495.
(33) Bottani, E. J. *Langmuir* **1999**, *15*, 5574.
(34) Chihara, K.; Suzuki, M.; Kawazoe, K. *J. Colloid Interface. Sci.* **1978**, *64*, 584.
(35) Steele, W. A. *Surf. Sci.* **1973**, *36*, 317.
(36) Harding, A. W.; Foley, N. J.; Norman, P. R.; Francis, D. C.; Thomas, K. M. *Langmuir* **1998**, *14*, 3858.
(37) Fletcher, A. J.; Thomas, K. M. *Langmuir* **1999**, *15*, 6908.
(38) Fletcher, A. J.; Thomas, K. M. *Langmuir* **2000**, *16*, 6253.
(39) Fletcher, A. J.; Cussen, E. J.; Prior, T. J.; Rosseinsky, M. J.; Kepert, C. J.; Thomas, K. M. *J. Am. Chem. Soc.* **2001**, *123*, 10001.